

Structural transformations in Pb/Si(111) phases induced by C₆₀ adsorption

This article has been downloaded from IOPscience. Please scroll down to see the full text article.

2013 J. Phys.: Condens. Matter 25 395006

(<http://iopscience.iop.org/0953-8984/25/39/395006>)

View [the table of contents for this issue](#), or go to the [journal homepage](#) for more

Download details:

IP Address: 109.70.248.5

The article was downloaded on 10/09/2013 at 16:22

Please note that [terms and conditions apply](#).

Structural transformations in Pb/Si(111) phases induced by C₆₀ adsorption

A V Matetskiy^{1,2}, L V Bondarenko^{1,2}, D V Gruznev^{1,2}, A V Zotov^{1,2,3},
A A Saranin^{1,2} and M C Tringides⁴

¹ Institute of Automation and Control Processes FEB RAS, 690041 Vladivostok, Russia

² School of Natural Sciences, Far Eastern Federal University, 690950 Vladivostok, Russia

³ Department of Electronics, Vladivostok State University of Economics and Service,
690600 Vladivostok, Russia

⁴ Ames Laboratory-USDOE and Department of Physics and Astronomy, Iowa State University, Ames,
IA 50011, USA

E-mail: saranin@iacp.dvo.ru

Received 24 April 2013, in final form 12 August 2013

Published 9 September 2013

Online at stacks.iop.org/JPhysCM/25/395006

Abstract

Structural transformations at the Pb/Si(111) surface occurring upon C₆₀ adsorption onto Pb/Si(111) 1 × 1 phase at room temperature and Pb/Si(111) $\sqrt{7} \times \sqrt{3}$ at low temperatures between 30 and 210 K, have been studied using scanning tunneling microscopy and low-energy electron diffraction observations. Typically, C₆₀ fullerenes agglomerate into random molecular islands nucleated at the surface defects. C₆₀ island formation is accompanied by expelling Pb atoms to the surrounding surface area where more dense Pb/Si(111) phases form. Productivity of C₆₀-induced expelling of Pb atoms is controlled by surface defects and is suppressed dramatically when regular ('crystalline') C₆₀ islands self-assemble at the defect-free Pb/Si(111) surface. When Pb atoms are ejected by the random C₆₀ islands, extended structural transformations involving reordering of numerous Pb atoms are fully completed at the surface within the shortest possible time (a few dozen seconds) to reapproach and image the surface after C₆₀ deposition. Estimations show that the observed transformations cannot be controlled by random walk diffusion of Pb adatoms, which implies a highly correlated motion of the Pb atom displacements within the layer.

(Some figures may appear in colour only in the online journal)

1. Introduction

Interaction of the large molecules, e.g., fullerenes, with solid surfaces can be quite sophisticated involving not only the effects of substrate on the structure and properties of forming molecular layers, but also restructuring of the substrate surface induced by molecular adsorption. In particular, on surfaces of various noble metals (e.g., Au [1–4], Pt [5–8], Ag [9–11], and Cu [12, 13]) adsorbed C₆₀ creates nanopits (vacancies) in the surface below the fullerenes. Up to seven metal atoms can be expelled by a fullerene, as in the case of Cu(111) surface [12]. The driving force leading to nanopit formation is associated with enhancing C₆₀-substrate bonding when the fullerene is partially embedded in the metal substrate and has more metal atom neighbors. The process is usually

triggered upon heating the sample to ~200–550 °C. Mass transport due to the C₆₀-induced pit formation manifests itself by the nucleation of metal islands on the surface [10–13]. Recently, a similar behavior has been detected for C₆₀ adsorption onto the In/Si(111) reconstructions [14, 15] where adsorbed C₆₀ fullerenes displace In atoms to the surrounding surface area to form domains of more dense In/Si(111) phases. The C₆₀-induced expulsion of In has been attributed to an inspiration of C₆₀ to change a relatively modest bonding with In metal layer to a stronger bond with the Si(111) substrate.

One can expect a similar phenomenon for C₆₀ adsorption onto Pb/Si(111) surfaces which are known to represent a set of various one-atomic-layer Pb phases on bulk-like Si(111) having various structures and Pb densities. The set includes, in particular, $\sqrt{7} \times \sqrt{3}$ [16], 1 × 1 [17],

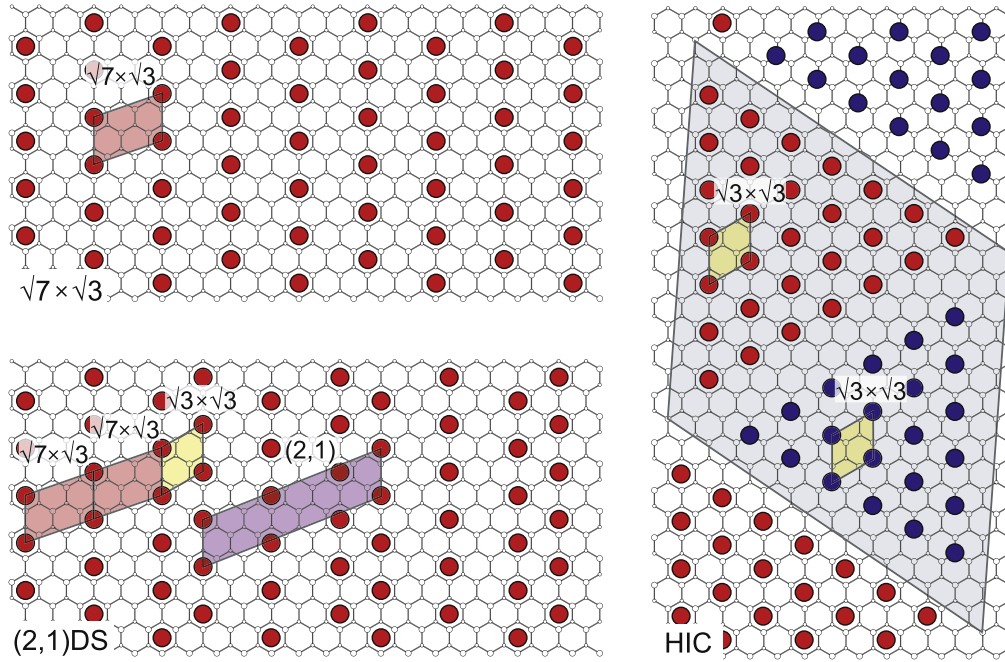


Figure 1. Schematic representation of the unit cells of three of the ordered phases discussed: the $\sqrt{7} \times \sqrt{3}$, the (2, 1) and the HIC A phases. The $\sqrt{7} \times \sqrt{3}$ and (2, 1) are DS linear phases with ordering along the $[1\bar{1}0]$ direction. The HIC A phase is built from $\sqrt{3}$ triangular domains with six-fold symmetry twisted off the $[1\bar{1}2]$ directions.

hexagonal incommensurate (HIC), striped incommensurate (SIC) $\alpha\text{-}\sqrt{3} \times \sqrt{3}$ [18, 19], and ‘devil’s staircase’ (DS) [20] phases. The DS phases are of especial interest bearing in mind that the formation of DS in systems with long-range repulsive interactions is one of the outstanding predictions in statistical mechanics. A key signature of a DS is the formation of a large number of ordered phases within a narrow coverage range, built hierarchically in complex patterns out of two generating phases, according to well-defined combinatorial rules. Sixteen such phases were discovered in Pb/Si(111) within the coverage range $6/5 \text{ ML} < \Theta_{\text{Pb}} < 4/3 \text{ ML}$ which is one of the best realizations of a DS in nature [20, 21]. This discovery has also settled many open questions about the system in the literature [22]. The formation of the DS phases is a result of the elastic interactions that become stronger with increasing Pb coverage. The two generating phases are the $\sqrt{7} \times \sqrt{3}$ with $\Theta_1 = 6/5 \text{ ML}$ and the $\sqrt{3} \times \sqrt{3}$ phase with $\Theta_2 = 4/3 \text{ ML}$ denoted as $\sqrt{7}$ and $\sqrt{3}$, respectively, and shown in figure 1. The DS phases of variable periodicity are built from $n\sqrt{7}$ and $m\sqrt{3}$ unit cells, denoted as the (n, m) phase. Along $[1\bar{1}0]$ the length of the $\sqrt{7}$ phase is $5a_0/2$ and the length of the $\sqrt{3}$ is $3a_0/2$ with a_0 the lattice constant of Si(111), so the period of the (n, m) phase is $(5n + 3m)a_0/2$ and its coverage $\Theta = (6n + 4m)/(5n + 4m)$. With heating, the linear (n, m) phases transform into phases of different symmetry, the hexagonal HIC and striped SIC phases [20–22].

It is worth noting, however, that no pit formation and Pb ejection have been noticed upon formation of C_{60} monolayer on Pb(111) (at least, at 120°C) [23] or upon room-temperature (RT) adsorption of individual C_{60} onto Pb/Si(111) 1×1 surface [24]. But if it was to occur under appropriate conditions, it could provide a valuable

atomic-scale information for clarifying the puzzling ultrafast mass transport phenomena detected recently in the Pb/Si(111) layers [25–27].

Results of the present low-energy electron diffraction (LEED) and scanning tunneling microscopy (STM) observations have demonstrated that C_{60} adsorbed onto Pb/Si(111) 1×1 at room temperature (RT) or Pb/Si(111) $\sqrt{7} \times \sqrt{3}$ at low temperatures (LT = 30–210 K) agglomerate into random molecular islands nucleated preferentially at defect sites. C_{60} island formation is accompanied by expulsion of Pb atoms to the surrounding surface area where more dense Pb/Si(111) phases are formed (i.e., HIC and SIC phases at RT and DS phases at LT). Even at temperatures as low as 30–110 K, no Pb adatoms are ever seen on top of the layer and domains of the newly formed DS phases after the Pb ejection are fully completed within the shortest possible time (a few dozen seconds) to reapproach and image the surface after C_{60} deposition. This indicates highly correlated motion of the Pb atom displacements within the layer. This suggests the observed transformations cannot be controlled by random walk diffusion of Pb adatoms.

2. Experimental details

Our experiments were performed with a variable-temperature Omicron STM operating in an ultrahigh vacuum ($\sim 7.0 \times 10^{-11}$ Torr). Atomically clean Si(111) 7×7 surfaces were prepared *in situ* by flashing to 1280°C , after the samples were first outgassed at 600°C for several hours. Lead (Pb) and C_{60} fullerenes were deposited from resistively heated Ta and Mo crucibles, respectively. For STM observations, electrochemically etched tungsten tips cleaned by *in situ*

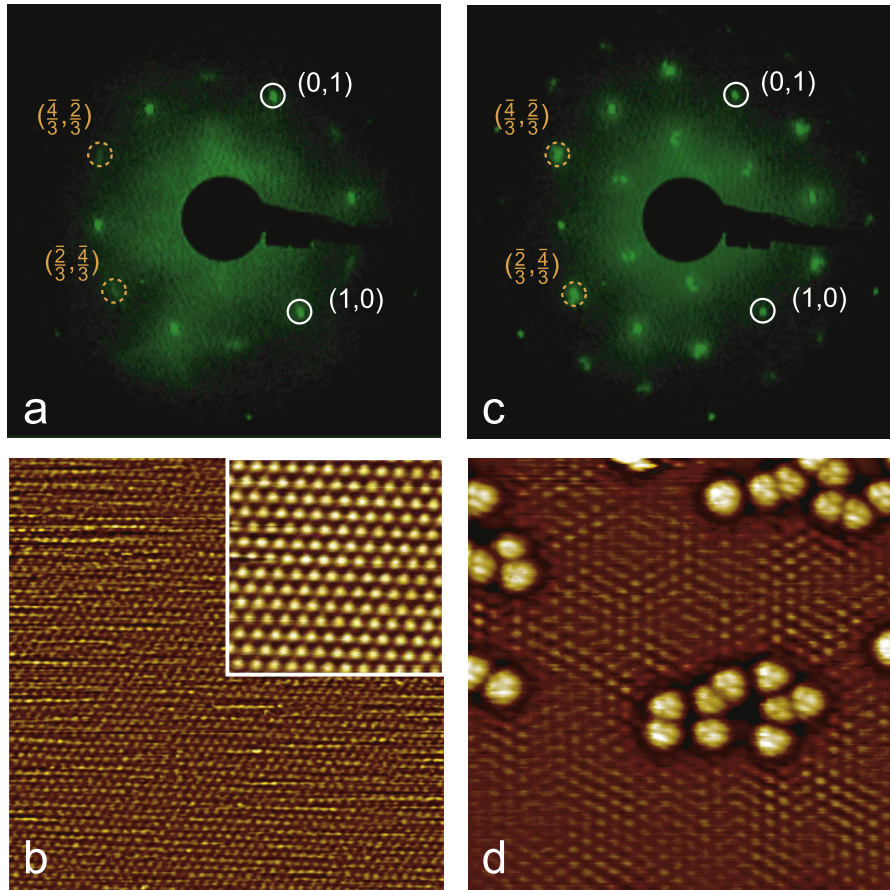


Figure 2. Result of RT C_{60} adsorption onto Pb/Si(111) 1×1 surface. (a) LEED pattern ($E = 74$ eV) and (b) $200 \times 200 \text{ \AA}^2$ STM image from the original Pb/Si(111) 1×1 surface. Inset shows the 1×1 structure at a greater magnification (scale: $50 \times 50 \text{ \AA}^2$). (c) LEED pattern ($E = 74$ eV) and (d) $200 \times 200 \text{ \AA}^2$ STM image from the surface after adsorption of 0.015 ML of C_{60} . The surface between C_{60} islands displays the HIC structure. The main reflections and $\sqrt{3}$ extra spots are indicated in the LEED patterns by solid white and dashed orange circles, respectively.

heating were employed. The experimental STM images shown in the paper were processed using high-pass FFT filtering to visualize the surface structure in between the fullerenes.

3. Results and discussion

3.1. C_{60} interaction with Pb/Si(111) surface

Figure 2 illustrates the structural transformation occurring at Pb/Si(111) surface upon RT adsorption of 0.015 ML of C_{60} . (1 ML (monolayer) = $7.8 \times 10^{14} \text{ cm}^{-2}$, the topmost Si atom density at non-reconstructed Si(111) 1×1 surface.) The original surface corresponds to the Pb/Si(111) 1×1 phase as evidenced by LEED and STM (figures 2(a) and (b)). The surface was prepared by RT deposition of ~ 1.2 ML of Pb followed by annealing at 200°C for 1 min. After such a preparation, the surface was almost completely covered by 1×1 phase with very seldom inclusions of small $\beta\text{-}\sqrt{3} \times \sqrt{3}$ domains (with $1/3$ ML of Pb). The above ‘overheating’ was specially done to minimize the uncontrolled amount of Pb adatoms present at the surface at RT. Indeed, cooling this

surface to low temperatures (e.g., below 270 K) converts 1×1 structure to pure $\sqrt{7} \times \sqrt{3}$ without any domains of DS phase present. Note that features of $\beta\text{-}\sqrt{3} \times \sqrt{3}$ structure are faintly present in the RT LEED pattern in figure 2(a). According to the reported phase diagram [19], the thus-prepared surface contains slightly less (due to presence of a small number of small $\beta\text{-}\sqrt{3} \times \sqrt{3}$ domains) than exactly 1.20 ML, the coverage of the $\sqrt{7} \times \sqrt{3}$, but this minute fraction is not involved in the transformations described in the current work. After RT adsorption of 0.015 ML of C_{60} the surface structure changes for $\alpha\text{-}\sqrt{3} \times \sqrt{3}$ HIC phase [18, 19] as evidenced by LEED and STM (figures 2(c) and (d)). The LEED observations prove that transformation takes place globally over the whole surface and are not associated with any tip effects which cannot be ruled out safely when one is limited by sole STM observations. Since HIC phase is known to contain ~ 1.25 ML of Pb [19], one obtains an estimate that each C_{60} fullerene (0.015 ML) expels on average $(1.25\text{--}1.20)/0.015 \sim 3$ Pb atoms. The ejection rate of the Pb atoms by C_{60} is a function of both the surface defect density and temperature. At low temperature the defects play the major role (as will be shown below) but at RT C_{60} islands nucleate also at defect-free regions with Pb ejection possible

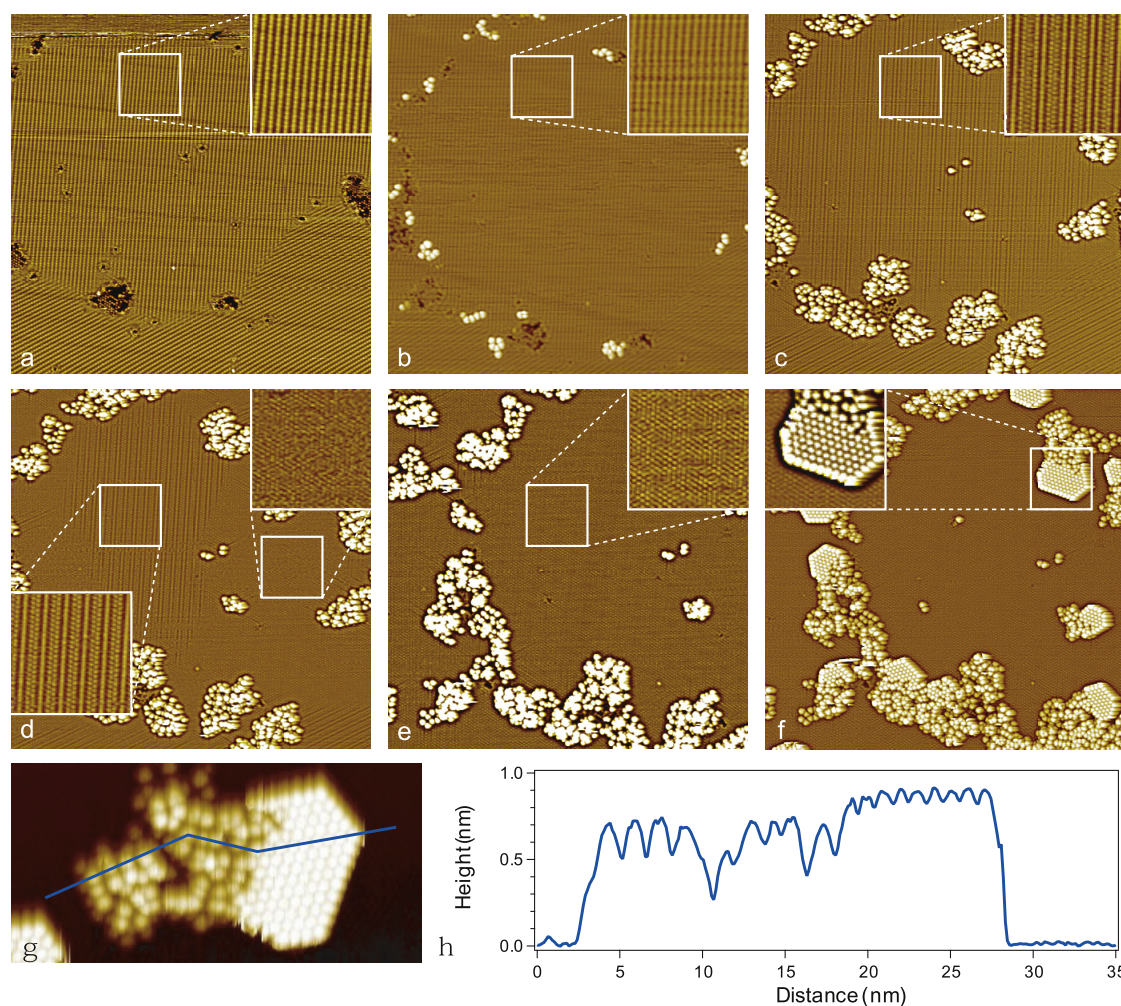


Figure 3. Sequence of $1000 \times 1000 \text{ \AA}^2$ STM images acquired from the same surface region (a) before C_{60} deposition and after depositing (b) 0.0015 ML, (c) 0.0075 ML, (d) 0.010 ML, (e) 0.012 ML, and (f) 0.019 ML of C_{60} . Insets show the structure of the outlined regions at a greater magnification. C_{60} deposition and STM image acquisition were conducted at 210 K. (h) STM profile along the line in (g) showing the height difference of C_{60} fullerenes in the ‘crystalline’ and random C_{60} islands.

even at these regions. One can notice that the C_{60} molecules in figure 2(d) have a characteristic three-lobe appearance which means that they are tightly bonded to the substrate in an orientation with a hexagon on top. The STM height profile analysis shows that the apparent height of such a C_{60} is only $\sim 4 \text{ \AA}$ above the HIC surface, indicating that the fullerenes are embedded into the Pb layer and bound to the Si(111) substrate.

As mentioned above, cooling the Pb/Si(111) 1×1 surface to LT transforms it to Pb/Si(111) $\sqrt{7} \times \sqrt{3}$ phase. As an example, figure 3(a) shows an STM image of such a surface. The image displays a large $\sqrt{7} \times \sqrt{3}$ domain surrounded by a circle-like domain boundary containing, in particular, structural defects (most of which originate from small inclusions of $\beta\text{-}\sqrt{3} \times \sqrt{3}$ phase). Figures 3(b)–(f) demonstrate the structural transformations occurring in this surface region with C_{60} deposition. One can see that C_{60} islands are mostly random in shape and nucleate preferentially at the surface defects indicating that the adsorbed C_{60} are free to migrate on bare Pb/Si(111) $\sqrt{7} \times \sqrt{3}$ surface over distances of, at the least, $\sim 50 \text{ nm}$ at 210 K. At the initial stage of C_{60} deposition (e.g., at 0.0015 ML of C_{60} , as in figure 3(b)), the $\sqrt{7} \times \sqrt{3}$ surface

remains essentially unchanged. However, after deposition of 0.0075 ML of C_{60} (figure 3(c)) the whole domain area converts mostly to (3, 1) DS phase having Pb coverage of 1.2222 ML [20]. At 0.010 ML of C_{60} (figure 3(d)), the (2, 1) DS phase with 1.2307 ML of Pb fills the interior of the domain and the HIC phase starts to develop at the domain rim. At 0.012 ML of C_{60} (figure 3(e)), the HIC phase having 1.25 ML Pb occupies the whole surface. With further C_{60} deposition (e.g., at 0.019 ML of C_{60} , as in figure 3(f)) the HIC phase remains unchanged. Meanwhile, the newly formed C_{60} islands adopt an ordered ‘crystalline’ structure instead of the random shape typical of the earlier stages of C_{60} deposition. This behavior is similar to that reported for C_{60} adsorbed onto In monoatomic layers on Si(111) [14] where fullerenes were unable to dig into the most dense In layer (i.e., the so-called quasi-rectangular $\text{rec-}\sqrt{7} \times \sqrt{3}$ -In reconstruction) and agglomerate into ‘crystalline’ islands on its top. Another essential feature of this stage is that all defective regions are already occupied by C_{60} and the remaining Pb/Si(111) is free of surface defects. Line profile analysis demonstrates that C_{60} fullerenes in the ‘crystalline’ islands are $\sim 2 \text{ \AA}$ higher than

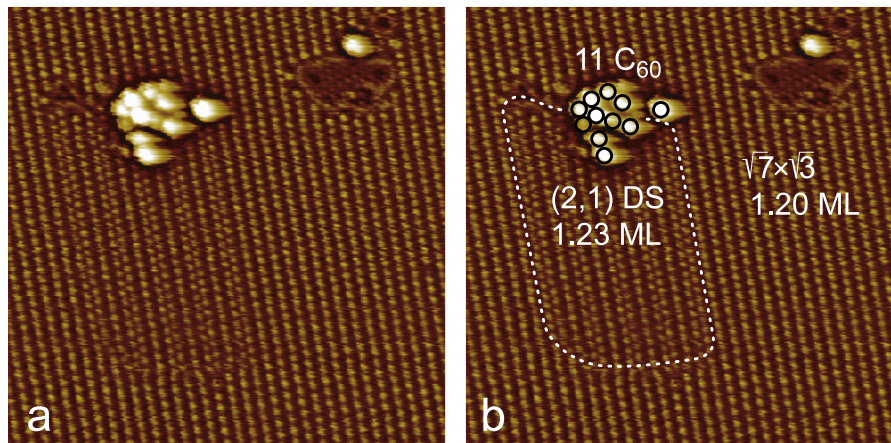


Figure 4. Effect produced by a given C_{60} island on the structure of the surrounding Pb/Si(111) surface region. (a) $315 \times 315 \text{ \AA}^2$ STM image of the random C_{60} island formed at the defected area upon C_{60} deposition onto Pb/Si(111) $\sqrt{7} \times \sqrt{3}$ surface held at 110 K. (b) The same image is shown again in which 11 C_{60} fullerenes forming the island and the surface area where transformations from original $\sqrt{7} \times \sqrt{3}$ structure with 1.20 ML Pb to the (2, 1) DS phase with 1.23 ML Pb takes place are outlined.

fullerenes in the random islands (figures 3(g) and (h)), which observation supports the assumption that the ‘crystalline’ islands are located atop the Pb layer while C_{60} in the random islands are embedded into the Pb layers. It is worth noting also that ‘crystalline’ islands adopt various azimuth orientations without apparent relation to the surface lattice. This probably indicates that van der Waals interaction between C_{60} in the ‘crystalline’ island prevails over C_{60} interaction with a HIC surface.

To monitor the effect produced by a single C_{60} island, we carried experiments over a lower temperature range of 30–110 K. As an example, figure 4(a) shows how formation of the island containing 11 C_{60} fullerenes induces the transformation in the adjacent area converting its structure from $\sqrt{7} \times \sqrt{3}$ to (2, 1) DS phase (i.e., Pb coverage increases from 1.20 to 1.2307 ML). From the area of the transformed region (which equals $\sim 233 \text{ nm}^2$ or $\sim 1824 \text{ Si(111)}1 \times 1$ unit cells), one obtains that the region adopts $(1.2307 - 1.20) \times 1824 \sim 56$ additional Pb atoms, hence each of 11 C_{60} fullerenes in the island expels ~ 5 Pb atoms in average. Consideration of the transformed area for the numerous C_{60} islands has shown that productivity of a C_{60} fullerene (i.e., the number of Pb atoms expelled by a given C_{60}) varies from 0 to 10 depending on the particular island. Most likely this is a consequence of the fact that C_{60} islands nucleate at the surface defects which have various atomic arrangements. Moreover, C_{60} fullerenes occupy non-equivalent sites within an island as evidenced by the difference in their apparent heights. As a result, each C_{60} can expel very different numbers of Pb atoms.

Experiments with the adsorption of small amounts of C_{60} onto the Pb/Si(111) surface which contains such a low density of defects that it looks almost defect-free have revealed that the presence of defects plays a key role for Pb atom extraction by C_{60} fullerenes. The C_{60} islands forming on the defect-free surface differ substantially from the islands nucleated at the defects. First, the C_{60} islands on the defect-free surface display regular (‘crystalline’) close-packed arrays of C_{60}

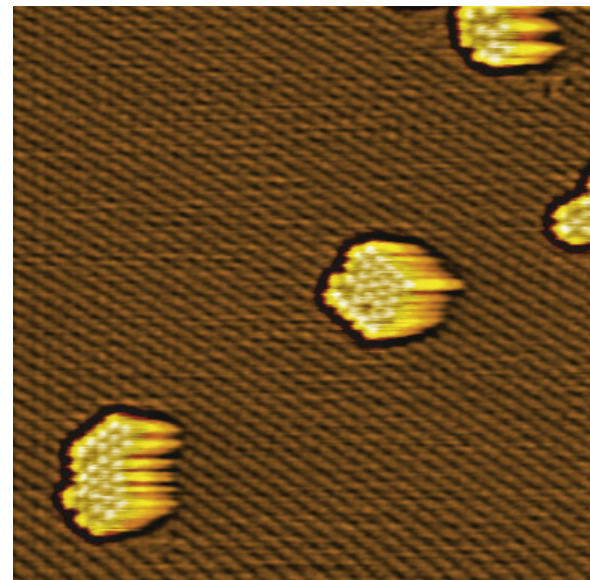


Figure 5. $245 \times 245 \text{ \AA}^2$ STM image showing self-assembled C_{60} islands nucleated at the defect-free Pb/Si(111) $\sqrt{7} \times \sqrt{3}$ surface at 95 K. The islands have a regular (‘crystalline’) structure of close-packed arrays of C_{60} having the same apparent heights. The original $\sqrt{7} \times \sqrt{3}$ surface structure around islands remains intact indicating that no Pb atoms are expelled by C_{60} .

having equivalent heights (figure 5), which is in contrast to the random C_{60} islands at the defects (figure 4(a)) but similar to the ‘crystalline’ islands which develop when all defective regions are already occupied (figure 3(f)). Second, C_{60} molecule in the ‘crystalline’ islands have an apparent height of $\sim 9 \text{ \AA}$ over $\sqrt{7} \times \sqrt{3}$ -Pb surface which implies that they reside atop the Pb layer. Third, C_{60} island bonding to the defect-free surface is much weaker than that to the surface defects: the latter islands are always stable while the former are sensitive to the tip effects. Such a behavior resembles that of C_{60} adsorbed onto inert surfaces, e.g. graphene [28], where island formation is driven mostly by the intermolecular

van der Waals interaction. Fourth, when a regular island self-arranges at the defect-free surface at low temperature, no structural transformations occur in the surrounding Pb/Si(111) region, indicating that no Pb atoms are expelled by C_{60} there. Thus, one can conclude that the surface defects are not only the preferential sites for C_{60} island nucleation but also the places where C_{60} -induced expulsion of Pb atoms is strongly facilitated (at least, at low temperatures). However, irrespective of the details of the ejection process, after local coverage increases, the transformation to the next DS phase is practically completed by the collection time of the next STM image.

3.2. Ultrafast structure reordering at the Pb/Si(111) surface

In addition to the study of the Pb ejection rate after C_{60} deposition, as already noted, it is remarkable that the pattern formation of the DS phases is completed at such low temperatures. This shows a novel type of collective mass transport. Collective processes have been found in other systems, with nanoislands and nanoscale complex patterns built exceedingly fast [29–33, 25, 26, 34]. The competition between the energy cost of domain boundaries and long-range elastic interactions in Pb/Cu(111) results in intricate patterns at 900 K of droplets or meandering stripes [29]. In Pb/Ge(111) [30] the low-temperature dense β - $\sqrt{3} \times \sqrt{3}$ phase with $\Theta = 4/3$ ML and the high-temperature disordered 1×1 phase, phase separate within several ms after cooling the system below the coexistence line. In other systems, such as Au/W(110) [31] and Pd/W(110) [32], where domain pattern formation is controlled by the competition between strain and domain wall energy, the domain pattern persists over much longer time after the critical temperature is reached.

In addition to the lower temperatures for Pb/Si(111) several other effects have been related to this unusually fast mass transport. It has been shown that growth at higher coverage ($\Theta > 1.5$ ML) is controlled by quantum size effects which lead to preferred island heights, with odd heights stable and even island heights unstable. Originally the non-classical and exceedingly fast mass transport was observed in coarsening experiments with surface x-ray scattering [33]. These results were further studied in the STM [25] and LEEM [26] experiments which have revealed the remarkable properties of the Pb wetting layer. The wetting layer moves in a superdiffusive motion $x \propto t$ (instead of $x \propto t^{1/2}$ expected from classical random walk motion). This fast moving wetting layer is the same as the α - $\sqrt{3} \times \sqrt{3}$ and DS phases shown to form exceedingly fast in the current C_{60} experiments.

A more recent experiment with LEEM [27] has shown an even more intriguing and unexpected result about the collective nature of the motion. Extending the experiment of [26] over the macroscopic distance ~ 0.1 mm it was observed that the refilling of the initially vacant area not only follows $x \propto t$ and is non-dispersive, but a second coverage discontinuity is observed propagating in the opposite direction to the inward moving refilling front. The motion of the two

fronts is highly correlated with the mass generated at the outwards moving front appearing at the inward refilling one in a mechanism reminiscent of the very fast formation of the DS phases in the current C_{60} experiments. In [27] whole DS rows extending over mesoscopic distances between the two moving fronts seemingly slide coherently similar to the way the DS rows form so quickly only on one side of the C_{60} islands. These unusual results about collective diffusion have also been seen in Pb/Ni(111) [34]. Theoretically work has been carried out to address the question of superdiffusive motion but there is still no clear understanding as to its origin [35–40].

The results from the present study complement the unusual mass transport results obtained with other techniques and provide a clear local picture of the speed and efficiency of the atomistic processes involved. As noted previously, these include: no diffusing adatoms seen on top of the layer, the DS rows are practically completed (within the shortest time ~ 100 s to collect the STM image as in figure 3 or to record the LEED pattern in figure 2) and the DS rows mysteriously develop only on one side of the C_{60} island (figure 4).

Within the previous discussion, the C_{60} experiments can be further analyzed to show more quantitatively how classical diffusion is ruled out to be responsible for the observed pattern formation. The LEED study of figure 2 shows how after depositing 0.015 ML of C_{60} the Pb/Si(111) 1×1 RT phase which has 1.20 ML Pb changes to the HIC phase which has 1.25 ML after the production of Pb adatoms. This is an even more elaborate transformation than the change from $\sqrt{7} \times \sqrt{3}$ to linear phase because the affected area is bigger and because the arrangements to form a hexagonal out of a linear phase involve more extended adatom correlations. As discussed before [18], the HIC phase is built from $\sqrt{3} \times \sqrt{3}$ unit cells on the interior of triangular domains and the $\sqrt{7} \times \sqrt{3}$ phase at the ‘corridors’ separating the triangular domains. The transformed area must be at least as large as the coherence length of the LEED diffractometer, $l \sim 40$ nm, since a well-developed diffraction pattern of the HIC phase is observed.

We can estimate the time needed for a Pb adatom starting somewhere randomly within the transformed area and at the last stage of the transformation to reach a specific location within the domain. This time will be shorter than the time to build the HIC phase since many more Pb adatoms should have diffused already to complete the transformation. If diffusion was a classical random walk this last adatom has many possible trajectories to follow in 2D, to start from an initial position and reach a final position different from the site dictated by the new pattern. But if we assume that the diffusing adatom is only performing a 1D random walk within the $[11\bar{2}]$ ‘corridors’ (which are at the boundaries of the HIC domains), this probability to reach the final position will be overestimated. Even with this restrictive favorable assumption, it will be seen that a stochastic uncorrelated random walk cannot account for the speed of the transformations at such low temperatures. Because both assumptions of 1D random walk and considering only the last Pb adatom to form the HIC phase underestimate τ , they will overestimate the diffusion activation energy E of single adatom hops.

We can take as the average distance of the diffusing Pb adatom the radius of this transformed area $l/2 \sim 50$ sites (since its initial position can be anywhere within the ‘corridor’). The probability of this adatom to reach a specific location in the shortest possible time is $p = (1/2)^{50}$ and the time to reach the final position within the HIC pattern is $(p\nu_0 \exp(-E/kT))^{-1}$; therefore this time must be less than the experimental time 100 s for LEED pattern acquisitions in figure 2 showing how the 1×1 transforms to the HIC phase after C_{60} deposition. Using a normal prefactor $\nu_0 = 10^{13} \text{ s}^{-1}$ this implies that $(1.1 \times 10^{16}) \times 10^{-13} \exp(E/kT) < 100$, so $\exp(E/kT) < 0.1$ which gives $E = -8.2 \text{ meV}$ at $T = 40 \text{ K}$ a negative activation energy.

This simple estimate, based on the motion of individual Pb adatoms moving stochastically, indicates that the formation of the new HIC pattern over at least the area of size l error-free (so a well-developed LEED pattern forms) is highly unlikely. A novel collective process must be operating whereby the incorporation of the Pb adatoms and the transport to the correct final site is done in a highly correlated way.

4. Conclusions

In conclusion, the current experiments have shown primarily how the C_{60} interaction on metal-covered semiconductor surface operates at such unusually low temperatures of 30–200 K to eject Pb adatoms and how defects in the substrate enhance the extraction process. Despite the low temperature the extraction of the Pb atoms leads to the formation of perfect DS phases in times limited by the data acquisition speed. This further illuminates the atomistic mechanisms operating on the recently discovered collective diffusion processes that result to efficient self-organization. Further theoretical work is needed to understand why C_{60} is so efficient in extracting Pb adatoms and what is the origin of the correlations and the self-organization in the Pb/Si(111) wetting layer.

Acknowledgments

Part of this work was supported by the Russian Foundation for Basic Research (Grant Nos 13-02-00837, 12-02-31832, 11-02-98515 and 11-02-98516), the Ministry of Education and Science of the RF (Grant Nos 8022, 8581 and 2.1004.2011) and Nsh-774.2012, the Office of Science, Basic Energy Sciences, Materials Sciences and Engineering Division of the US Department of Energy (USDOE), under Contract No. DEAC0207CH11358 with the US Department of Energy.

References

- [1] Zhang X, Yin F, Palmer R E and Guo Q 2008 The $C_{60}/\text{Au}(111)$ interface at room temperature: a scanning tunneling microscopy study *Surf. Sci.* **602** 885–92
- [2] Gardener J A, Briggs G A D and Castell M R 2009 Scanning tunneling microscopy studies of C_{60} monolayers on $\text{Au}(111)$ *Phys. Rev. B* **80** 235434
- [3] Tang L, Zhang X, Guo Q, Wu Y-N, Wang L-L and Cheng H-P 2010 Two bonding configurations for individually adsorbed C_{60} molecules on $\text{Au}(111)$ *Phys. Rev. B* **82** 125414
- [4] Hinterstein M, Torrelles X, Felici R, Rius J, Huang M, Fabris S, Fuess H and Pedio M 2008 Looking underneath fullerenes on $\text{Au}(110)$: formation of dimples in the substrate *Phys. Rev. B* **77** 153412
- [5] Felici R, Pedio M, Borgatti F, Iannotta S, Capozzi M, Ciullo G and Stierle A 2005 X-ray-diffraction characterization of $\text{Pt}(111)$ surface nanopatterning induced by C_{60} adsorption *Nature Mater.* **4** 688–92
- [6] Liu C, Qin Z, Chen J, Guo Q, Yu Y and Cao G 2011 Molecular orientations and interfacial structure of C_{60} on $\text{Pt}(111)$ *J. Chem. Phys.* **134** 044707
- [7] Torrelles X, Langlais V, De Santis M, Tolentino H C N and Gauthier Y 2010 Nanostructuring surfaces: deconstruction of the $\text{Pt}(110)$ - (1×2) surface by C_{60} *Phys. Rev. B* **81** 041404
- [8] Torrelles X, Langlais V, De Santis M, Tolentino H C N and Gauthier Y 2010 Nanoscale patterning by C_{60} ordering on $\text{Pt}(110)$ *J. Phys. Chem. C* **114** 15645–52
- [9] Li H I et al 2009 Surface geometry of C_{60} on $\text{Ag}(111)$ *Phys. Rev. Lett.* **103** 056101
- [10] Pai W W and Hsu C-L 2003 Ordering of an incommensurate molecular layer with adsorbate-induced reconstruction: $C_{60}/\text{Ag}(100)$ *Phys. Rev. B* **68** 121403
- [11] Hsu C-L and Pai W W 2003 Aperiodic incommensurate phase of a C_{60} monolayer on $\text{Ag}(100)$ *Phys. Rev. B* **68** 245414
- [12] Pai W W et al 2010 Optimal electron doping of a C_{60} monolayer on $\text{Cu}(111)$ via interface reconstruction *Phys. Rev. Lett.* **104** 036103
- [13] Pai W W, Hsu C-L, Lin M C, Lin K C and Tang T B 2004 Structural relaxation of adlayers in the presence of adsorbate-induced reconstruction: $C_{60}/\text{Cu}(111)$ *Phys. Rev. B* **69** 125405
- [14] Gruznev D V, Matetskiy A V, Gvozdi I V, Zotov A V and Saranin A A 2011 C_{60} adsorption onto the one-atomic-layer in films on $\text{Si}(111)$ surface *Surf. Sci.* **605** 1951–5
- [15] Kotlyar V G, Olyanich D A, Utas T V, Zotov A V and Saranin A A 2012 Self-assembly of C_{60} fullerenes on quasi-one-dimensional $\text{Si}(111)4 \times 1$ -In surface *Surf. Sci.* **606** 1821–4
- [16] Švec M, Cháb V and Tringides C 2009 Resolving the coverage puzzle of the $\text{Pb}/\text{Si}(111)-\sqrt{7} \times \sqrt{3}$ phase *J. Appl. Phys.* **106** 053501
- [17] Choi W H, Kim K S and Yeom H W 2008 High-energy core-level photoemission study of dense Pb overlayers on $\text{Si}(111)$ *Phys. Rev. B* **78** 195425
- [18] Hupalo M, Chan T L, Wang C Z, Ho K M and Tringides M C 2002 Atomic models, domain-wall arrangement, and electronic structure of the dense $\text{Pb}/\text{Si}(111)-\sqrt{3} \times \sqrt{3}$ phase *Phys. Rev. B* **66** 161410
- [19] Stepanovsky S, Yakes M, Yeh V, Hupalo M and Tringides M C 2006 The dense $\alpha-\sqrt{3} \times \sqrt{3}$ $\text{Pb}/\text{Si}(111)$ phase: a comprehensive STM and SPA-LEED study of ordering, phase transitions and interactions *Surf. Sci.* **600** 1417–30
- [20] Hupalo M, Schmalian J and Tringides M C 2003 Devil’s staircase in $\text{Pb}/\text{Si}(111)$ ordered phases *Phys. Rev. Lett.* **90** 216106
- [21] Yakes M, Hupalo M, Zaluska-Kotur M A, Gortel Z W and Tringides M C 2007 Low-temperature ultrafast mobility in systems with long-range repulsive interactions: $\text{Pb}/\text{Si}(111)$ *Phys. Rev. Lett.* **98** 135504
- [22] Tong X, Horikoshi K and Hasegawa S 1999 Structure and electrical conductance of Pb-covered $\text{Si}(111)$ surfaces *Phys. Rev. B* **60** 5653–8
- [23] Li H I, Franke K J, Pascual J I, Bruch L W and Diehl R D 2009 Origin of Moiré structures in C_{60} on $\text{Pb}(111)$ and their effect on molecular energy levels *Phys. Rev. B* **80** 085415
- [24] Chang S H, Hwang I S, Fang C K and Tsong T T 2008 Adsorption and motion of C_{60} molecules on the Pb-covered $\text{Si}(111)$ surface *Phys. Rev. B* **77** 155421

- [25] Hupalo M and Tringides M C 2007 Ultrafast kinetics in Pb/Si(111) from the collective spreading of the wetting layer *Phys. Rev. B* **75** 235443
- [26] Man K L, Tringides M C, Loy M M T and Altman M S 2008 Anomalous mass transport in the Pb wetting layer on the Si(111) surface *Phys. Rev. Lett.* **101** 226102
- [27] Man K L, Tringides M C, Loy M M T and Altman M S 2013 Superdiffusive motion of the Pb wetting layer on the Si(111) surface *Phys. Rev. Lett.* **110** 036104
- [28] Švec M, Merino P, Dappe Y J, González C, Abad E, Jelínek P and Martín-Gago J A 2012 Van der Waals interactions mediating the cohesion of fullerenes on graphene *Phys. Rev. B* **86** 121407
- [29] Plass R, Last J A, Bartelt N C and Kellogg G L 2001 Nanostructures: self-assembled domain patterns *Nature* **412** 875
- [30] Sato Y, Chiang S and Bartelt N C 2007 Spontaneous domain switching during phase separation of Pb on Ge(111) *Phys. Rev. Lett.* **99** 096103
- [31] de la Figuera J, Léonard F, Bartelt N C, Stumpf R and McCarty K F 2008 Nanoscale periodicity in stripe-forming systems at high temperature: Au/W(110) *Phys. Rev. Lett.* **100** 186102
- [32] Mentş T O, Locatelli A, Aballe L and Bauer E 2008 Stress induced stripe formation in Pd/W(110) *Phys. Rev. Lett.* **101** 085701
- [33] Jeffrey C A, Conrad E H, Feng R, Hupalo M, Kim C, Ryan P J, Miceli P F and Tringides M C 2006 Influence of quantum size effects on island coarsening *Phys. Rev. Lett.* **96** 106105
- [34] Bollmann T R J, van Gastel R, Zandvliet H J W and Poelsema B 2011 Anomalous decay of electronically stabilized lead mesas on Ni(111) *Phys. Rev. Lett.* **107** 136103
- [35] Huang L, Wang C Z, Li M Z and Ho K M 2012 Coverage-dependent collective diffusion of a dense Pb wetting layer on Si(111) *Phys. Rev. Lett.* **108** 026101
- [36] Krack B D, Ozoliņš V, Asta M and Daruka I 2002 Devil's staircases in bulk-immiscible ultrathin alloy films *Phys. Rev. Lett.* **88** 186101
- [37] Uche O U, Perez D, Voter A F and Hamilton J C 2009 Rapid diffusion of magic-size islands by combined glide and vacancy mechanism *Phys. Rev. Lett.* **103** 046101
- [38] Howe J D, Bhopale P, Tiwary Y and Fichthorn K A 2010 Patterns in strained-layer heteroepitaxy: beyond the Frenkel–Kontorova model *Phys. Rev. B* **81** 121410
- [39] Elder K R, Rossi G, Kanerva P, Sanches F, Ying S-C, Granato E, Achim C V and Ala-Nissila T 2012 Patterning of heteroepitaxial overlayers from nano to micron scales *Phys. Rev. Lett.* **108** 226102
- [40] Granato E and Ying S C 2012 Evolution of non-equilibrium profile in adsorbate layer under compressive strain *Tribol. Lett.* **48** 83–8